Neutral Möbius [5]helicene-embedded Cycloparaphenylene Nanohoops: Synthesis, [4n]Möbius Topology and Hückel Aromaticity

Huiji Yang, Shengzhu Guo, Weijie Guo, Xiaoyu Liu, Jing He, Yanqing Fan, Zhe Lian, Xiaonan Li, Ying Wang,* Hua Jiang*

College of Chemistry, Beijing Normal University, Beijing 100875 (P. R. China).

KEYWORDS. Möbius topology, aromaticity, nanohoop, helicene, circularly polarized luminescence

ABSTRACT: The relationship between Möbius topology and aromaticity and topological chirality is still elusive to date, which is, to a large extent, due to the related synthetic challenges and, further, the scarcity in both the quantity and the diversity of the constructed Möbius systems. In this work, we reported the synthesis of [4n]Möbius conjugated all-carbon nanohoops (**[5]H-[7,8]CPPs**) by utilizing a [5]helicene unit as a hidden writhe and a masked aromatic unit to overcome the strain inherited from Möbius topology. X-ray analysis revealed that **[5]H-[7,8]CPPs** contain a [5]helicene moiety and an oligoparaphenylene unit, and display a Möbius topology. Photophysical investigations demonstrated that **[5]H-[7,8]CPPs** exhibited moderately high fluorescence quantum yields, which are significantly higher than those of pristine [5]helicene and [7,8]CPPs. Chiroptical studies revealed that **[5]H-[7,8]CPPs** displayed an obvious Cotton effect in circular dichroism and bright circularly polarized luminescence, indicating that the chirality of [5]helicene was efficiently transferred to the overall carbon nanohoops. Importantly, theoretical investigations reveal that, though possessing a 4n π-electron array, such all-carbon nanohoops are fully conjugated systems with Hückel aromaticity. The results may help us to better understand the relationship between Möbius topology and aromaticity.

Introduction

The research on aromaticity and stability of cyclic π-conjugated systems with distinct topology has attracted much attention of both organic and theoretic chemists, and received a significant evolution in synthesis and theory since the landmark discovery of benzene by Faraday in 1825. [1-5] It is well recognized that annulenes displaying a Hückel topology are aromatic and stable when their cyclic conjugated π-electrons are 4n+2, whereas those with 4n are antiaromatic and unstable. However, when annulene is twisted by 180° to adopt a Möbius topology that is the classic example of a non-orientable surface, its electronic structure and aromatic character were changed significantly. The concept of Möbius aromaticity, proposed by Heilbronner in 1964, predicted that Möbius annulenes with 4n conjugated π-electrons should be aromatic and stable. [6] Since then, annulenes with a Möbius topology have aroused tremendous interest to both synthetic organic and theoretic chemists. One of important milestones in the field of Möbius aromaticity was demonstrated by the first successful synthesis of a [16] Möbius annulene by Herges and co-workers in 2003, [7] and followed by the expanded porphyrin with a dynamic Möbius-Hückel aromaticity. [8] After that, the topic of Möbius aromaticity has been mainly dominated by expanded porphyrinoid systems because their structural features can potentially stabilize Möbius aromatic systems. [9-11]

Stimulated by recent advances on all-carbon nanoarchitectures with distinct topologies such as catenanes, knots and rotaxanes, [12-21] conjugated all-carbon nanohoops with a Möbius topology have recaptured great attention of scientists from synthetic organic chemistry, physical science and material science. So far, there are limited examples of Möbius conjugated all-carbon nanohoops because of the synthetic difficulties associated with the twisted topological structure. [3-5] In 2014, Herges and co-workers reported the first triply twisted Möbius [24]dehydroannulene, [22] whose conjugation is interrupted by large torsional angles due to its flexible building blocks. Durola and Herges then developed a triple cyclic tri-[5]helicenes with a Möbius topology, exhibiting a strong diatropic ring current in the outer periphery. However, no net macrocyclic aromaticity was displayed due to the counterbalance of the diatropic and paratropic currents in the outer π and the inner σ system, respectively. [23] Moore and co-workers reported the synthesis of a Möbius tris((ethynyl)[5]helicene) macrocycle showing no significant global aromaticity due to the weak conjugation between the alkyne and adjacent helicene units. [24] Cong and Zhu disclosed the aromaticity of mechanically interlocked Möbius conjugated nanohoops. [25] Šolomek reported a Möbius nanohoop containing [6]helicene unit with circularly polarized luminescence. [26] Unfortunately, this nanohoop lacks the basis for Möbius aromaticity studies because the presence of [6]helicene in nanohoop leads to an odd number of π-electrons in the cyclic conjugated pathway. Very recently, a Möbius topology has been disclosed in the twisted [n]cycloparaphenylene with alkene insertion by Kayahara and Yamago. [27] Besides above excellent advances, there are a few elegant examples on other aromatic macrocycles with a Möbius topology. [28-30] Nevertheless, the relationship between Möbius topology and aromaticity/chirality, in particular if there is inevitable connection between [4n]Möbius topology and Möbius aromaticity, is still far from being fully understood.

We have a long-term interest in conjugated carbon nanohoops [31-36]. Herein, we present the design and synthesis of [4n]Möbius conjugated all-carbon nanohoops by hybridization of [5]helicene (Figure 1 and Scheme 1) and cycloparaphenylenes as well as their Möbius topologies. We demonstrated that the presence of [5]helicene unit in [7,8]cycloparaphenylenes enable the conjugated all-carbon nanohoops to exhibit a Möbius topology with [4n] π-electrons in the cyclic conjugated pathway and bright circularly polarized luminescence. More importantly, the Möbius nanohoops are aromatic, which are supported by the results of Nucleus-independent chemical shifts (NICS), harmonic oscillator model of aromaticity (HOMA), Anisotropy of the induced current density (AICD) and localized orbital locator-π/σ (LOL-π/σ) calculations.

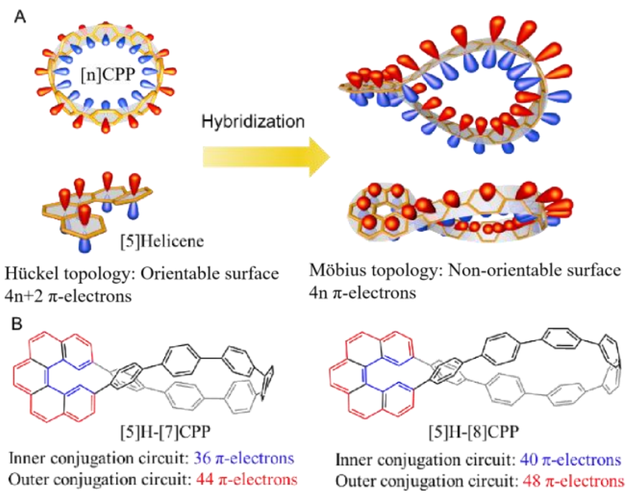

Figure 1. (A) Concept of this work: the cartoon illustration of hybridization of two conjugated subunits ([5]helicene and cycloparaphenylene) with a Hückel topology into a globally conjugated carbon nanohoop with a Möbius topology. (B) the structures of the [4n]Möbius conjugated all-carbon nanohoops studied herein. Each nanohoop contains two different conjugated circuits dependent on the inner (blue) or outer (red) paths of helicene. All cyclic conjugation paths contain 4n π-electrons.

Results and discussion

Design and Synthesis

In a singly twisted Möbius annulene featuring a molecular twist and an overall macrocyclic conjugation (Figure 1), a 180° twist induces strain in π-conjugated macrocycle and thus causes tremendous difficulties in stabilizing the Möbius topology. The utilization of a hidden writhe such as helicene to circumvent this difficulty has been successfully demonstrated in helicene-based Möbius annulenes. [23, 24, 26] However, this method is not yet enough to mitigate strain caused by the overall macrocyclic conjugation within a singly twisted Möbius annulene. On the other hand, a 3,6-*syn*-dimethoxy-cyclohexa-1,4-diene moiety as a masked aromatic ring has been successfully used to develop strained [n]cycloparaphenylenes ([n]CPPs) followed by sequential aromatization. [37]

We envisaged that this masked aromatic ring could be utilized to construct marginally strained macrocyclic Möbius precursor in combination with [5]helicene as a hidden writhe, and sequential aromatization of the cyclohexadiene units in macrocyclic Möbius precursor would readily build up strained Möbius conjugated all-carbon nanohoop. More importantly, the presence of [5]helicene subunit in Möbius conjugated carbon nanohoops eventually provide the cyclic conjugation paths with 4n π-electrons (Figure 1 B), that is, **[5]H-[7]CPP** contains 44 and 36 π electrons in the peripheric and inner conjugation circuits, respectively; for **[5]H-[8]CPP**, those are 48 and 40 ones, respectively, which are ready for investigating the relationship between [4n]Möbius topology and aromaticity in present work.

The synthetic routes to **[5]H-[7]CPP** and **[5]H-[8]CPP** are outlined in Scheme 1. The targeted Möbius nanohoop **[5]H-[7]CPP** was synthesized by Suzuki-Miyaura cross-coupling between dibromopentahelicene **1** [38] and C-shaped synthon **2**, [39] followed by a reductive aromatization in 20% yield over two steps. In the case of **[5]H-[8]CPP,** compound **4** was generated in a yield of 80% by Suzuki coupling reaction between **1** and 4-chlorophenylboronic acid, and was then converted to borate ester **5** in a yield of 85%. Compound **7** was obtained by the Suzuki coupling reaction of **5** with L-shaped synthon **6** in

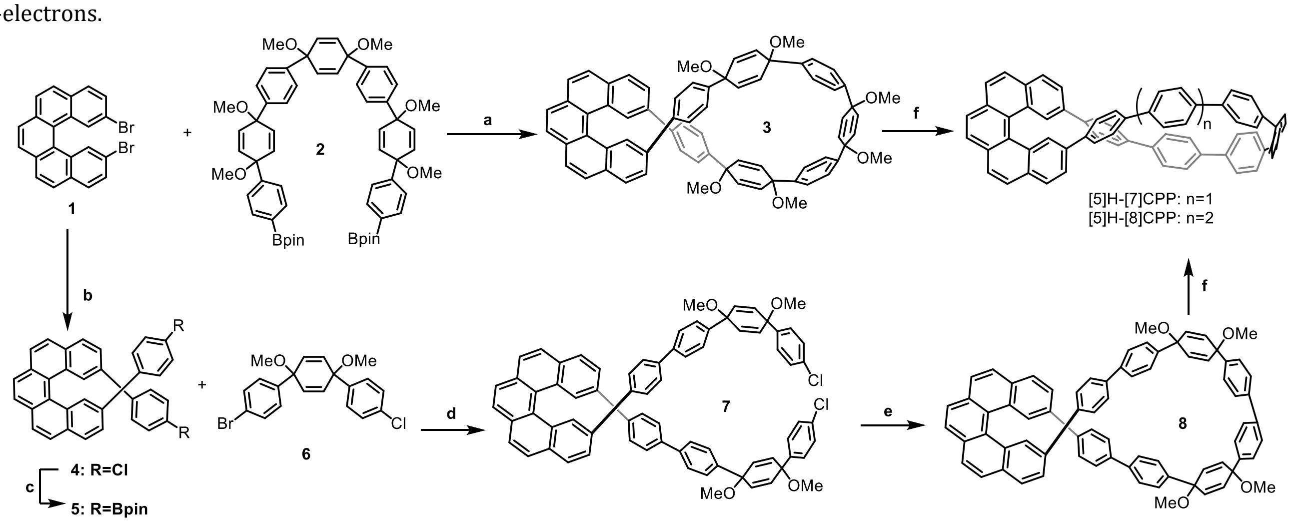

Scheme 1. Synthesis of **[5]H-[7, 8]CPP**. (a) 2M NaOH, $Pd(PPh_3)_4$, 1,4-dioxane, H_2O, 115 °C, overnight, crude compound; (b) 4-Chlorophenyboronic acid, 2M $CsCO_3$, $Pd(PPh_3)_4$, 1,4-dioxane, H_2O, 115 °C, overnight, 80%; (c) X-phos, $Pd_2(dba)_3$, B_2pin_2, KOAc, 1,4-dioxane, 115 °C, overnight, 85%; (d) 2M K_2CO_3, $Pd(PPh_3)_4$, 1,4-dioxane, H_2O, 115 °C, overnight, 72%; (e) bpy, $Ni(COD)_2$, THF, 75 °C, overnight; (f) H_2SnCl_4, THF, RT, overnight, 20% for **[5]H-[7]CPP** and 35% for **[5]H-[8]CPP**.

https://doi.org/10.26434/chemrxiv-2024-vxf63 **ORCID:** https://orcid.org/0000-0002-9917-2683 Content not peer-reviewed by ChemRxiv. **License:** CC BY-NC-ND 4.0

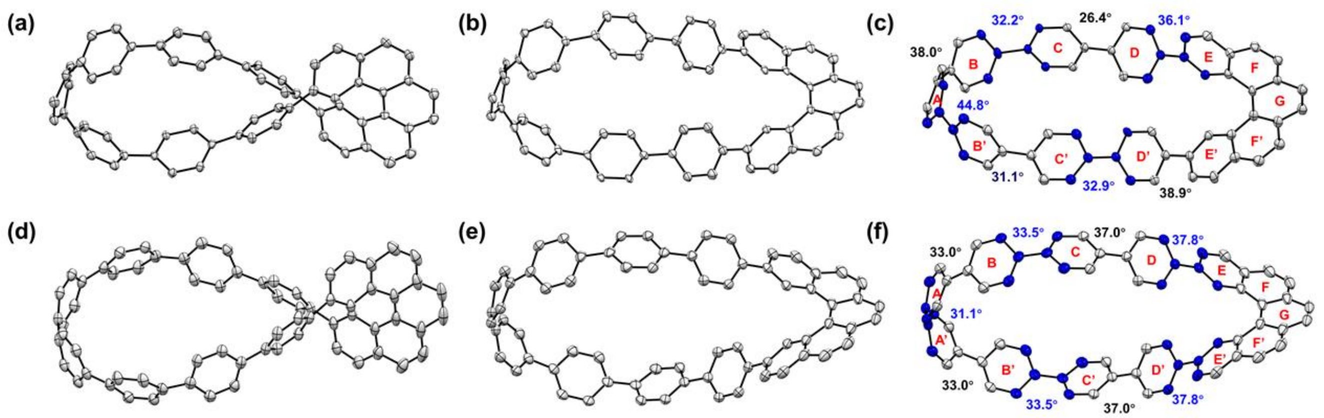

Figure 2. X-ray crystal structures of the target compounds: a) the side view, b) the top view, c) the dihedral angles of **[5]H-[7]CPP.** d) the side view, e) the top view, f) the dihedral angles of **[5]H-[8]CPP**. Only *P*-enantiomers are shown.

the presence of $Pd(PPh_3)_4$, 2M K_2CO_3 in deoxygenated 1,4-dioxane and H_2O in a yield of 72%. Precursor **8** was obtained by a ring-closure reaction via a nickel-mediated Yamamoto reaction without further purification, [40-41] subjected to a reductive aromatization using freshly made H_2SnCl_4 in anhydrous THF at room temperature to afford the final Möbius nanohoop **[5]H-[8]CPP** as a yellow solid in a total yield of 35%.

Crystallography

The single crystals of **[5]H-[7]CPP** were obtained by slowly volatilizing a chloroform solution at 4 °C, while the single crystals of **[5]H-[8]CPP** were obtained by crystalizing its solution in a mixture of DCM/toluene (1:1, v/v) at 4 °C. The single crystal X-ray analysis showed that **[5]H-[7]CPP** was crystallized in triclinic *P1* space group, while **[5]H-[8]CPP** was solved in orthorhombic *Pnna* space group. In each case, two pairs of enantiomers were found in each unit cell. As shown in **Figure 2**, the crystal structures clearly demonstrate that **[5]H-[7]CPP** and **[5]H-[8]CPP** possess a Möbius topology with a reasonable overall conjugation. For **[5]H-[7]CPP**, the dihedral angles of the adjacent benzenes are found to be from 26.4° to 44.8°, while those for **[5]H-[8]CPP** are from 31.1° to 38.7° (Figure 2c and 2f). The fluctuated extent of the dihedral angles for **[5]H-[7]CPP** is larger than those for **[5]H-[8]CPP,** mainly due to its larger strain in **[5]H-[7]CPP,** which is supported by DFT calculations (*vide infra*). The dihedral angles of **[5]H-[7]CPP** and **[5]H-[8]CPP** in the solid phases are in good agreement with those predicted by DFT (b3lyp/6-31g(d)/PCM-UFF) symmetry-unconstrained calculations (Figure S2-S3). The same arguments also hold for the torsional angles (Figure S4-S5, Table S2-S3). These dihedral and torsional angles are relatively small, thus allowing the structures of **[5]H-[7]CPP** and **[5]H-[8]CPP** to satisfy the criteria of Möbius aromaticity asserted by Rzepa. [4, 42]

The strain energies of the Möbius nanohoops were estimated by DFT calculations according to the homodesmotic reactions shown in Scheme S2, wherein the nanohoops and biphenyl are converted to diphenyl[5]helicenes and terphenyl. The strain energies of **[5]H-[7]CPP** and **[5]H-[8]CPP** are calculated to be 52.5 and 47.8 kcal mol^{-1}, respectively, which indicates that **[5]H-[7]CPP** is less stable due to the smaller nanohoop size as expected. Such strain energies of **[5]H-[7]CPP** and **[5]H-[8]CPP** are close to those of [11]CPP (54 kcal mol^{-1}) and [12]CPP (48 kcal mol^{-1}), but are significantly smaller than those of [7]CPP (84 kcal mol^{-1}) and [8]CPP (72 kcal mol^{-1}), [43] respectively, indicating that the presence with [5]helicene moiety substantially decrease the tension of [n]CPP nanohoops possessing the same number of paraphenylene units. Moreover, it is worth noting that the strain energy of **[5]H-[7]CPP** is smaller than that (55.4 kcal mol^{-1}) of Šolomek's [6]helicene nanohoop with the same numbers of paraphenylene units, [26] implying that the [5]helicene nanohoops are more stable.

Absorption and emission properties

The photophysical properties of **[5]H-[7]CPP** and **[5]H-[8]CPP** were examined by UV–vis and fluorescence spectroscopies and the photophysical parameters are summarized in Table 1 and S5. As shown in Figure 3, **[5]H-[7]CPP** displays a main absorption peak at 332 nm with a molar extinction coeffecient (ε) of 1.0×10^4 M^{-1} cm^{-1} and a shoulder band in the range of 370 to 450 nm. **[5]H-[8]CPP** displays a similar absorption contour to that of **[5]H-[7]CPP** but with a much larger ε of $2.6{\times}10^4$ $M^{-1}cm^{-1}$ at 332 nm. The maximum absorption peaks of **[5]H-[7]CPP** and **[5]H-[8]CPP** are slightly blue-shifted as compared with those of [7-8]CPPs, presumably due to the presence of [5]helicene in the cyclic conjugations.

The fluorescence emissions of **[5]H-[7,8]CPP** were measured in DCM solution. **[5]H-[7,8]CPP** emit strong fluorescence with a main peak at about 490 nm, which is red-shifted by 60 nm when compared with [5]helicene (λ_{em}= 430 nm) but significantly blue-shifted by 93 and 43 nm relative to [7,8]CPPs, respectively. The fluorescence quantum yields (Φ_F) were determined to be 37.1% for **[5]H-[7]CPP** and 44.6% for **[5]H-[8]CPP**, which are moderate but significantly higher than those of the pristine [7-8]CPPs [19] and [5]helicene. [46-47] The symmetry breaking caused by the presence of [5]helicene moiety in the nanohoops is partially responsible for the turn-on fluorescence of [5]helicene-based nanohoops. [48] The enhancement in fluorescence quantum yields were further interpreted by theoretic calculations (*vide infra*). The fluorescence lifetimes (τ) of **[5]H-[7]CPP** and **[5]H-[8]CPP** were found to be 3.0 ns and 3.1 ns by single-exponential decay fitting (Figure. S8), respectively. The radiative decay rate constants (k_r) were corresponded to be 1.24×10^8 s^{-1} for **[5]H-[7]CPP** and 1.44×10^8 s^{-1} for **[5]H-[8]CPP**, respectively.

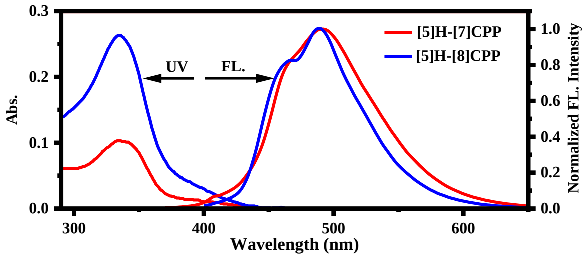

Figure 3. UV/Vis absorption and fluorescence emission spectra of [5]H-[7]CPP (red) and [5]H-[8]CPP (blue) in CH_2Cl_2 (1.0×10^{-5} M).

Table 1. Photophysical properties of [5]H-[7]CPP [a], [5]H-[8]CPP [a], [7]CPP [44], [8]CPP [45] and [5]Helicene [46-47].

Compd.	λ_{Abs}[b] /nm	$\varepsilon_m\times10^4$	λ_{em} [c]/nm	Φ_F[d]/ %	τ/ns
[5]H-[7]CPP	332	1.0	490	37.1	3.0
[5]H-[8]CPP	332	2.6	490	44.6	3.1
[7]CPP	340	6.9	587	0.7	NA
[8]CPP	340	10.0	533	10	17.6
[5]Helicene	300	-	430	4	25.5

(a) UV-vis absorption and fluorescence spectra were measured in DCM (1.0×10^{-5} M) at room temperature. (b) Maximum absorption. (c) Maximum emission upon excitation at 332 nm. (d) Fluorescence quantum yields were measured by using a calibrated integrating sphere, excited at 332 nm.

The frontier molecular orbitals (FMOs) calculated at DFT(b3lyp/6-31g(d) level reveal similar orbital characteristics for **[5]H-[7]CPP** and **[5]H-[8]CPP** (Figure 4 and S9). Both HOMO and LUMO mainly concentrate on the paraphenylene moieties, whereas HOMO-1 and LUMO+1 are comparatively more dispersed and mainly scattered over the [5]helicene subunits. The energy diagrams of the dominant excitations are shown in the left of Figure 4. In both cases, the absorption bands at 332 nm are mainly contributed to transitions from HOMO-2→LUMO+1 and HOMO→LUMO+4, which are corresponding to the calculated absorption maxima at 339 nm for **[5]H-[7]CPP** and 342 nm for **[5]H-[8]CPP**, respectively, with the large oscillator strength (*f*) values. The small shoulder bands around 400 nm are corresponding to the transition of HOMO→LUMO. Note that the FMOs of [5]helicene are no longer HOMOs and LUMOs of **[5]H-[7]CPP** and **[5]H-[8]CPP** so that the emission wavelength are mainly dependent on the cyclic paraphenylene units, which are presumably accountable for the fact that the fluorescence quantum yields of [5]helicene-based nanohoops are significantly higher than that of the pristine [5]helicene. **[5]H-[7]CPP** features the HOMO and the LUMO energy level of -5.23 and -1.76 eV, respectively, slightly higher than that of **[5]H-[8]CPP** corresponding to -5.48 and -2.12 eV, respectively (Figure 4). The HOMO–LUMO gaps of **[5]H-[7]CPP** and **[5]H-[8]CPP** are thus determined to be 3.46 and 3.35 eV, respectively, which are slightly narrower than those of [11]CPP and [12]CPP (3.53 and 3.63 eV, respectively). The HOMO–LUMO gap of **[5]H-[7]CPP** is larger than that of **[7]CPP** (3.17 eV). However, the HOMO–LUMO gap of **[5]H-[8]CPP** is comparable with that of [8]CPP (3.41 eV, b3lyp/6-31g(d) level). [49]

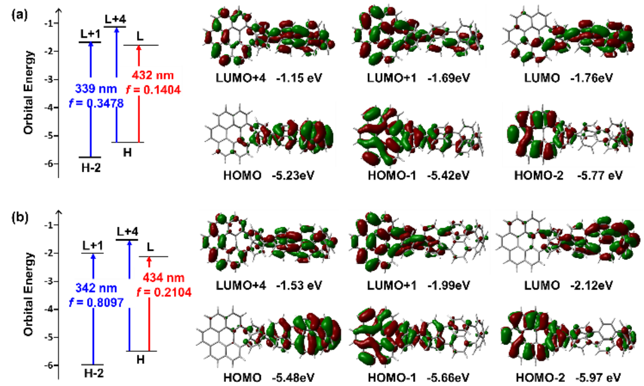

Figure 4. Energy diagrams and pictorial representations of the FMOs for [5]H-[7]CPP (a) and [5]H-[8]CPP (b). The values of f represent the oscillator strengths.

Chiroptical properties

Chiral resolutions of the enantiomers of **[5]H-[7]CPP** and **[5]H-[8]CPP** were achieved by HPLC with a chiral-stationary-phase column (Chiralpak IB column, 4.6 mm Φ × 250 mm L) and a UV detector, in which the mobile phase was DCM/n-heptane (40:60) with a flow of 2 mL/min. Each pair of enantiomers were obtained as a pair of isolated fractions with a ratio of about 1:1, respectively (Figure S12). The ECD spectra of the two isolated HPLC fractions recorded in DCM solution (Figure 5a and 5b) were perfect mirror images corresponding to the *P*- and *M*-enantiomers of **[5]H-[7]CPP** and **[5]H-[8]CPP,** respectively, which were assigned according to the computational studies (Figure S13). The ECD spectra of enantiomers display multiple Cotton effects in the range of 250 to 450 nm, with two distinct sign inversions at λ=310 and 374 nm for **[5]H-[7]CPP** and at λ=314 and 374 nm for **[5]H-[8]CPP** (Figure 5 and S14), respectively. The enantiomers of **[5]H-[7]CPP** exhibits a maximum CD signal at 350 nm with $|\Delta\varepsilon|$ = 20.1 $M^{-1}cm^{-1}$ and the $|g_{abs}|$ value of 2.4×10^{-3}, while the enantiomers of **[5]H-[8]CPP** also exhibits a maximum CD signal at the same wavelength but with a larger $|\Delta\varepsilon|$ = 74.3 $M^{-1}cm^{-1}$ and $|g_{abs}|$ value of 3.6×10^{-3} (Figure S15).

The chiroptical properties of the excited states were investigated by the means of circularly polarized luminescence (CPL) spectroscopy. The two enantiomers of **[5]H-[7]CPP** and **[5]H-[8]CPP** show CPL emission in the range of 425 to 625 nm (Figure 5), which are corresponding to the fluorescence emission. The CPL spectra of each pair of enantiomers are mirror images of each other. The maximum CPL dissymmetry factor ($|g_{lum}|$) can evaluate the magnitudes of CPL, thus the $|g_{lum}|$ values were determined to be 2.03 $\times10^{-3}$ and 1.47 $\times10^{-3}$ for **[5]H-[7]CPP** and **[5]H-[8]CPP**, respectively, which are in the range of 10^{-5} to 10^{-3} for small organic molecules. [50-54] The ratios of $|g_{lum}|$ and $|g_{abs}|$ were calculated to be 0.86 and 0.41 for **[5]H-[7]CPP** and **[5]H-[8]CPP**, respectively. The values are likely to indicate that the geometric change between the ground and excited states is little for **[5]H-[7]CPP** but significant for **[5]H-[8]CPP,** which is presumably due to that the structure in excited state of **[5]H-[7]CPP** is more rigid than that of **[5]H-[8]CPP**. [50-57]

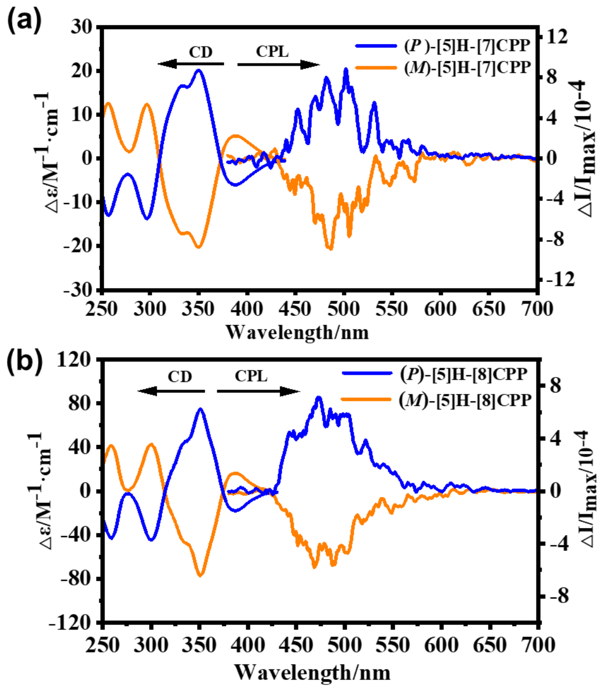

Figure 5. CD and CPL spectra of (a) [5]H-[7]CPP and (b) [5]H-[8]CPP in DCM (1.0×10^{-5}M).

Computational studies on aromaticity

Nucleus-independent chemical shifts (NICS) analysis has been extensively used for molecular aromaticity determination. The NICS(±1)$_{zz}$ values of all the six-membered rings of the studied neutral systems, obtained from the GIAO-b3lyp/6-31+g(d,p) computations, are largely negative (Figure S20-S21), thus indicating local Hückel aromaticity of these moieties. Geometric aromaticity analyses, on the basis of the structures optimized at the b3lyp 6-31+g(d,p) level, provided accordant results. In both **[5]H-[7]CPP** and **[5]H-[8]CPP**, the harmonic oscillator model of aromaticity (HOMA) values are determined to be 0.989-0.993 of the *p*-phenylene units, revealing that these rings are highly locally aromatic. values of about 0.950 of the peripheral rings and 0.84-0.89 for the rest ones in the [5]helicene moiety are obtained, which is due to the twisted conformation and the strong π-conjugation in this unit (Figure S22-S23, Table S9 and S10).

Interestingly, the calculated NICS$_{zz}$ values show the differences on the periphery and interior cavity of the Möbius nanohoops. For the ghost atoms located at the periphery of the nanohoop for a specific ring, the value is typically less negative compared to the corresponding one located inside (Figure S20-S21), suggestive of a more aromatic circumstance for the inner cavity of the nanohoops [58]. Further NICS-scan was carried out, in which the NICS probes were placed the inner cavity of the nanohoops at intervals of 2.61 and 2.91 Å to give a quinque-section in the case of **[5]H-[7]CPP** and **[5]H-[8]CPP**, respectively, along the theoretical C_2 axis of symmetry. As shown in **Figure 6, S20** and **S21**, ignoring place A that located in the bay area of the [5]helicene moiety, the NICS values at the inner cavity are in the range from -7.2 to -3.2 and from -9.8 to -4.0 ppm for **[5]H-[7]CPP** and **[5]H-[8]CPP**, respectively. These small negative NICS values could be due to the presence of marginal aromaticity and the small positive values of position A might be ascribed to the, comparatively, stronger paratropic current flowing in the bay of the helicene moiety.

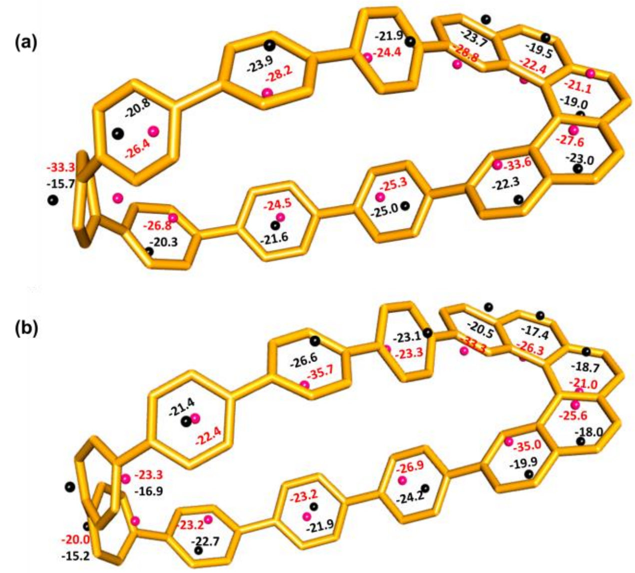

Figure 6. NICS(1)$_{zz}$ values of **[5]H-[7]CPP**and **[5]H-[8]CPP** calculated at GIAO-B3LYP/6-31+g(d,p) level of theory. The values of the ghost atoms corresponding to the outer periphery and cavity of the nanohoops are indicated in black and pink, respectively. Hydrogen atoms are omitted for clarity in the structures.

Anisotropy of the induced current density (AICD) analyses are widely accepted for visualization of aromaticity. [3, 22-25, 59-61] The AICD plot (isovalue = 0.50) of **[5]H-[7]CPP** (Figure S24) shows locally diatropic currents in each individual benzene ring. For the [5]helicene moiety, a strong diatropic current can be observed in the periphery and a paratropic current presents in the bay. Similar pattern is also observable in the case of **[5]H-[8]CPP**. Such AICD plots are strongly indicative of a Hückel-aromaticity for both **[5]H-[7]CPP** and **[5]H-[8]CPP**.

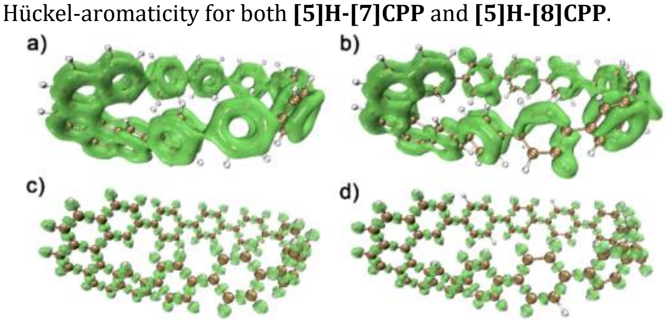

Figure 7. LOL-π isosurfaces (isovalue = 0.30) for (a) [5]H-[7]CPP and (b) [5]H-[8]CPP and that of LOL- σ (isovalue = 0.60) for (c) [5]H-[7]CPP and (d) [5]H-[8]CPP.

The isolated electron density observed in the localized orbital locator-π (LOL-π) plots [62-64] are in good agreement with the results of the NICS and AICD analysis as well (Figure 7). In the case of **[5]H-[7]CPP**, at isovalue = 0.30 level, the π-electrons delocalize over all the [5]helicene moiety and the individual benzene rings. Nevertheless, the π-electrons do not spread continuously in the whole [7]cycloparaphenylenes fragment, and bifurcations located at the bridging C–C single bonds are observed, indicating that the π-conjugation within **[5]H-[7]CPP** is not significant enough, inhibiting the system to display global aromaticity. For **[5]H-[8]CPP**, a similar, but less continuous, π-electrons delocalization pattern is shown, suggestive of a weaker electron conjugation. This phenomenon, similar to those of their parent molecules [n]CPPs, [44, 45, 49] is understandable because that a smaller nanohoop would give rise to a better radial π-overlap and thus an effective increase in the π-conjugation between the neighbouring aryl rings. Notably, LOL-σ plots at isovalue = 0.60 clearly show that the electrons delocalization on the C–C atoms bridged neighbouring aryls are comparable to that over the benzene rings, suggesting that **[5]H-[7]CPP** and **[5]H-[8]CPP** are still π-conjugated to some extent.

Conclusions

A convenient and modular synthetic strategy is developed for preparing conjugated all-carbon nanohoops with a Möbius topology by hybridizing [5]helicene and oligoparaphenylene units. X-ray structural analyses revealed that the conjugated all-carbon nanohoops exhibit a Möbius topology. The photophysical and chiroptical properties of the all-carbon nanohoops were investigated after HPLC resolutions. The all-carbon nanohoops display electronic circular dichroism with multi-bands and bright CPL emissions, with moderately high absorption and luminescence dissymmetry factors. Theoretical structural analysis revealed that the presence of [5]helicene unit leads to a significant mitigation of strain and the cyclic conjugated pathways with 4n π-electrons. The computational investigations revealed a weak conjugated, Hückel aromatic character for these neutral all-carbon nanohoops. Our findings reveal that there is no necessary connection between [4n]Möbius topology and Möbius aromaticity in the present case. We expected that cationic nanohoops of **[5]H-[7]CPP** and **[5]H-[8]CPP** may possess different aromatic characters compared to the neutral analogues. The effort on investigating Möbius aromaticity of these cationic species is undergoing in our lab and will be reported in due course.

ASSOCIATED CONTENT

Supporting Information.

The Supporting Information is available free of chargeathttps://pubs.acs.org/doi/xxx.

Experimental details, additional NMR, mass spectroscopy, as well as fluorescence titration experiments have been displayed at Supporting Information.

AUTHOR INFORMATION

Corresponding Author

Hua Jiang, College of Chemistry, Beijing Normal University, Beijing 100875 (P. R. China)

Ying Wang, College of Chemistry, Beijing Normal University, Beijing 100875 (P. R. China)

Notes

The authors declare no competing financial interest.

ACKNOWLEDGMENT

This work was financially supported by the National Natural Science Foundation of China (21971021, 22271019 and 22371018). We thank Dr. Di Sun at School of Chemistry and Chemical Engineering, Shandong University for assistance with crystal analysis.

Notes

The authors declare no competing financial interest.

REFERENCES

1 Garratt, P. J. *Aromaticity,* Wiley, **1986**, pp. 1-19.

2 Krygowsk, T. M.; Cyrański, M. K. Structural Aspects of Aromaticity. *Chem. Rev.* **2001**, 101, 1385-1419.

3 Herges, R. Topology in Chemistry: Designing Möbius Molecules. *Chem. Rev.* **2006**, 106, 4820-4842.

4 Rzepa, H. S. Möbius Aromaticity and Delocalization. *Chem. Rev.* **2005**, 105, 3697-3715.

5 Schaller, G. R.; Herges, R. Möbius molecules with twists and writhes. *Chem. Commun*. **2013**, 49, 1254.

6 Heilbronner, E. Hűckel molecular orbitals of Mőbius-type conformations of annulenes. *Tetrahedron Lett*. **1964**, 5, 1923–1928.

7 Ajami, D.; Oeckler, O.; Simon, A.; Herges, R. Synthesis of a Möbius aromatic hydrocarbon. *Nature.* **2003**, 426, 819-821.

8 Stępień, M.; Latos-Grażyński, L.; Sprutta, N.; Chwalisz, P.; Szterenberg, L. Expanded Porphyrin with a Split Personality: A Hückel–Möbius Aromaticity Switch. *Angew. Chem. Int. Ed*. **2007**, 46, 7869-7873.

9 Stępień, M.; Sprutta, N.; Latos-Grażyński, L. Figure Eights, Möbius Bands, and More: Conformation and Aromaticity of Porphyrinoids. *Angew. Chem. Int. Ed.* **2011**, 50, 4288-4340.

10 Saito, S.; Osuka, A. Expanded Porphyrins: Intriguing Structures, Electronic Properties, and Reactivities. *Angew. Chem. Int. Ed.* **2011**, 50, 4342-4373;

11 Yoon, Z. S.; Osuka, A.; Kim, D. Möbius aromaticity and antiaromaticity in expanded porphyrins. *Nat. Chem*. **2009**, 1, 113-122.

12 Segawa, Y.; Kuwayama, M.; Hijikata, Y.; Fushimi, M.; Nishihara, T.; Pirillo, J.; Shirasaki, J.; Kubota, N.; Itami, K. Topological molecular nanocarbons: All-benzene catenane and trefoil knot. *Science.* **2019**, 365, 272–276.

13 Raden, J. M. V.; White, B. M.; Zakharov, L. N.; Jasti, R. Nanohoop Rotaxanes from Active Metal Template Syntheses and Their Potential in Sensing Applications. *Angew. Chem. Int. Ed.* **2019**, 58, 7341 –7345.

14 Segawa, Y.; Levine, D. R.; Itami, K. Topologically Unique Molecular Nanocarbons. *Acc. Chem. Res.* **2019**, 52, 2760–2767.

15 Segawa, Y.; Kuwayama, M.; Itami, K. Synthesis and Structure of [9]Cycloparaphenylene Catenane: An All-Benzene Catenane Consisting of Small Rings. *Org. Lett.* **2020**, 22, 1067−1070.

16 Raden, J. M. V.; Jarenwattananon, N. N.; Zakharov, L. N.; Jasti, R. Active Metal Template Synthesis and Characterization of a Nanohoop [c2]Daisy Chain Rotaxane. *Chem. Eur. J.* **2020**, 26, 10205–1020.

17 Muramats, T.; Okado, Y.; Traeger, H.; Schrettl, S.; Tamaoki, N.; Weder, C.; Sagara, Y. Rotaxane-Based Dual Function Mechanophores Exhibiting Reversible and Irreversible Responses. *J. Am. Chem. Soc*. **2021**, 143, 9884−9892.

18 Zhang,X.; Shi, H.; Zhuang, G.; Wang, S.; Wang, J.; Yang, S.; Shao, X.; Du, P. A Highly Strained All-Phenylene Conjoined Bismacrocycle. *Angew. Chem. Int. Ed*. **2021**, 60, 17368 – 17372;

19 Zhang, X.; Liu, H.; Zhuang, G.; Yang, S.; Du, P. An unexpected dual-emissive luminogen with tunable aggregation-induced emission and enhanced chiroptical property. *Nat. Commun*. **2022**, 13, 3543;

20 Bu, A.; Zhao, Y.; Xiao, H.; Tung, C.-H.; Wu, L.-Z.; Cong, H. A Conjugated Covalent Template Strategy for All-Benzene Catenane Synthesis. *Angew. Chem. Int. Ed*. **2022**, 61, e202209449.

21 May, J. H.; Raden, J. M. V.; Maust, R. L.; Zakharov, L. N.; Jasti, R. Active template strategy for the preparation of π-conjugated interlocked nanocarbons. *Nat. Chem.* **2023**, 15, 170–176.

22 Schaller, G. R.; Topić, F.; Rissanen, K.; Okamoto, Y.; Shen, J.; Herges, R. Design and synthesis of the first triply twisted Möbius annulene. *Nat. Chem*. **2014**, 6, 608-613.
23 Naulet, G.; Sturm, L.; Robert, A.; Dechambenoit, P.; Röhricht, F.; Herges, R.; Bock, H.; Durola, F. Cyclic tris-[5]helicenes with single and triple twisted Möbius topologies and Möbius aromaticity. *Chem. Sci*. **2018**, 9, 8930–8936.
24 Jiang, X.; Laffoon, J. D.; Chen, D.; Pérez-Estrada, S.; Danis, A. S.; Rodríguez-López, J.; Garcia-Garibay, M. A.; Zhu, J.; Moore, J. S. Kinetic Control in the Synthesis of a Möbius Tris((ethynyl)[5]helicene) Macrocycle Using Alkyne Metathesis. *J. Am. Chem. Soc*. **2020**, 142, 6493-6498.
25 Fan, Y.-Y.; Chen, D.; Huang, Z.-A.; Zhu, J.; Tung, C.-H.; Wu, L.-Z.; Cong, H. An isolable catenane consisting of two Möbius conjugated nanohoops. *Nat. Commun*. **2018**, 9, 3037.
26 Malinčík, J.; Gaikwad, S.; Mora-Fuentes, J. P.; Boillat, M.; Prescimone, A.; Häussinger, D.; Campaña, A. G.; Šolomek, T. Circularly Polarized Luminescence in a Möbius Helicene Carbon Nanohoop. *Angew. Chem. Int. Ed*. **2022**, 61, e202208591.
27 Terabayashi, T.; Kayahara, E.; Zhang, Y.; Mizuhata, Y.; Tokitoh, N.; Nishinaga, T.; Kato, T.; Yamago, S. Synthesis of Twisted [n]Cycloparaphenylene by Alkene Insertion. *Angew. Chem. Int. Ed.* **2023**, 62, e202214960.
28 Nishigaki, S.; Shibata, Y.; Nakajima, A.; Okajima, H.; Masumoto, Y.; Osawa, T.; Muranaka, A.; Sugiyama, H.; Horikawa, A.; Uekusa, H.; Koshino, H.; Uchiyama, M.; Sakamoto, A.; Tanaka, K. Synthesis of Belt- and Möbius-Shaped Cycloparaphenylenes by Rhodium-Catalyzed Alkyne Cyclotrimerization. *J. Am. Chem. Soc*. **2019**, 141, 14955-14960.
29 Wang, S.; Yuan, J.; Xie, J.; Lu, Z.; Jiang, L.; Mu, Y.; Huo, Y.; Tsuchido, Y.; Zhu, K. Sulphur-Embedded Hydrocarbon Belts: Synthesis, Structure and Redox Chemistry of Cyclothianthrenes. *Angew. Chem. Int. Ed.* **2021**, 60, 18443-18447.
30 Segawa, Y.; Watanabe, T.; Yamanoue, K.; Kuwayama, M.; Watanabe, K.; Pirillo, J.; Hijikata, Y.; Itami, K. Synthesis of a Möbius carbon nanobelt. *Nat. Synth*. **2022**, 1, 535-541.
31 Guo, S.; Liu, L.; Su, F.; Yang, H.; Liu, G.; Fan, Y.; He, J.; Lian, Z.; Li, X.; Guo, W.; Chen, X.; Jiang, H. Monitoring Hierarchical Assembly of Ring-in-Ring and Russian-doll Complexes based on Carbon Nanoring by Förster Resonance Energy Transfer. *JACS Au*. **2024**, DOI: 10.1021/jacsau.3c00720.
32 Guo, S. Z.; Liu, L.; Li, X. N.; Liu, G. Q.; Fan, Y. Q.; He, J.; Lian, Z.; Yang, H. J.; Chen, X. B.; Jiang, H. Highly Luminescent Chiral Carbon Nanohoops via Symmetry Breaking with a Triptycene unit: Bright Circularly Polarized Luminescence and Size-dependent Properties. *Small*. **2023**, 2308429.
33 Fan, Y. -Q.; Fan, S.; Liu, L.; Guo, S. Z.; He, J.; Li, X. -N.; Lian, Z.; Guo, W. J.; Chen, X. B.; Wang, Y.; Jiang, H. Efficient Manipulating Förster Resonance Energy Transfer through Host-Guest Interaction Enables Tunable White-Light Emission and Devices in Heterotopic Bisnanohoops. *Chem. Sci.* **2023**, 14, 11121-11130.
34 Fan, Y. Q.; He, J.; Guo, S. Z.; Jiang, H. Host-Guest Chemistry in Binary and Ternary Complexes Utilizing π-Conjugated Carbon Nanorings. *ChemPlusChem.* **2023,** e202300536.
35 Fan, Y. Q.; He, J.; Liu, L.; Liu, G. Q.; Guo, S. Z.; Lian, Z.; Li, X. N.; Guo, W. J.; Chen, X. B.; Wang, Y.; Jiang, H. Chiral Carbon Nanorings: Synthesis, Properties and Hierarchical Self-assembly of Chiral Ternary Complexes Featuring a Narcissistic Chiral Self-Recognition for Chiral Amines. *Angew. Chem. Int. Ed.* **2023**, 62, e202304623.
36 He, J.; Yu, M.; Lian, Z.; Fan, Y. -Q.; Guo, S. Z.; Li, X. -N.; Wang, Y.; Wang, W. G.; Cheng, Z. -Y.; Jiang, H. Lemniscular carbon nanohoops with contiguous conjugation from planar chiral [2.2]paracyclophane: influence of the regioselective synthesis on topological chirality. *Chem. Sci.* **2023**, 14, 4426-4433.
37 Jasti, R.; Bhattacharjee, J.; Neaton, J. B.; Bertozzi, C. R. Synthesis, Characterization, and Theory of [9]-, [12]-, and [18]Cycloparaphenylene: Carbon Nanohoop Structures. *J. Am. Chem. Soc*. **2008**, 130, 17646-17647.
38 Jhulki, S.; Mishra, A. K.; Chow, T. J.; Moorthy, J. N. Helicenes as All-in-One Organic Materials for Application in OLEDs: Synthesis and Diverse Applications of Carbo- and Aza[5]helical Diamines. *Chem. Eur. J.* **2016**, 22, 9375-9386.
39 Wang, S.; Li, X.; Zhang, X.; Huang, P.; Fang, P.; Wang, J.; Yang, S.; Wu, K.; Du, P. A supramolecular polymeric heterojunction composed of an all-carbon conjugated polymer and fullerenes. *Chem. Sci.* **2021**, 12, 10506-10513.
40 Yamamoto, T.; Maruyama, T.; Zhou, Z.-H.; Ito, T.; Fukuda, T.; Yoneda, Y.; Begum, F.; Ikeda, T.; Sasaki, S.; Takezoe, H.; Fukuda, A.; Kubota, K. pi.-Conjugated Poly(pyridine-2,5-diyl), Poly(2,2'-bipyridine-5,5'-diyl), and Their Alkyl Derivatives. Preparation, Linear Structure, Function as a Ligand to Form Their Transition Metal Complexes, Catalytic Reactions, n-Type Electrically Conducting Properties, Optical Properties, and Alignment on Substrates. *J. Am. Chem. Soc.* **1994**, 116, 4832.
41 Yamamoto, T.; Anzai, K.; Fukumoto, H. Preparation of Soluble π-Conjugated Poly(5,6-dialkoxy-1,10-phenanthroline-3,8-diyl)s. Their Stacking Behavior and Function as a π-Conjugated Polymer Ligand. *Chem. Lett.* **2002**, 774-775.
42 Park, J. K.; Yoon, Z. S.; Yoon, M.-C.; Kim, K. S.; Mori, S.; Shin, J.-Y.; Osuka, A.; Kim, D. Möbius Aromaticity in N-Fused [24]Pentaphyrin upon Rh(I) Metalation. *J. Am. Chem. Soc*. **2008**, 130, 1824-1825.
43 Segawa, Y.; Omachi, H.; Itami, K. Theoretical studies on the structures and strain energies of cycloparaphenylenes. *Org. Lett.* **2010**, 12, 10, 2262–2265.
44 Segawa, Y.; Fukazawa, A.; Matsuura, S.; Omachi, H.; Yamaguchi, S.; Irle, S.; Itami, K. Combined experimental and theoretical studies on the photophysical properties of cycloparaphenylenes. *Org. Biomol. Chem.* **2012**, 10, 5979 and references therein.
45 Darzia, E. R.; Jasti, R. The dynamic, size-dependent properties of [5]–[12]cycloparaphenylenes. *Chem. Soc. Rev.*, **2015**, 44, 6401-6410.
46 Kubo, H.; Hirose, T.; Matsuda, K. Control over the Emission Properties of [5]Helicenes Based on the Symmetry and Energy Levels of Their Molecular Orbitals. *Org. Lett.* **2017**, 19, 1776–1779.
47 Birks, J. B.; Birch, D. J. S.; Cordemans, E.; Donckt, E. V. Fluorescence of the higher helicenes. *Chem. Phys. Lett.* **1976**, 43, 33–36.
48 Lovell, T. C.; Colwell, C. E.; Zakharovb, L. N.; Jasti, R. Symmetry breaking and the turn-on fluorescence of small, highly strained carbon nanohoops. *Chem. Sci*. **2019**, 10, 3786.
49 Iwamoto, T.; Watanabe, Y.; Sakamoto, Y.; Suzuki, T.; Yamago, S. Formation of SnO_2 Hollow Nanospheres inside Mesoporous Silica Nanoreactors. *J. Am. Chem. Soc.* **2011**, 133, 21, 8354-8361.
50 Sánchez-Carnerero, E. M.; Agarrabeitia, A. R.; Moreno, F., Maroto, B. L.; Muller, G.; Ortiz, M. J.; Moya, S. d. l. Circularly Polarized Luminescence from Simple Organic Molecules. *Chem. Eur. J.* **2015**, 21, 13488–13500.
51 Zheng, D.; Zheng, L.; Yu, C.; Zhan, Y.; Wang, Y.; Jiang, H. Significant Enhancement of Circularly Polarized Luminescence Dissymmetry Factors in Quinoline Oligoamide Foldamers with Absolute Helicity. *Org. Lett.* **2019**, 21, 2555–2559.
52 Zheng, D.; Yu, C.; Zheng, L.; Zhan, Y.; Jiang, H. Absolute control of helicity at the C-termini in quinoline oligoamide foldamers by chiral oxazolylaniline moieties. *Chin. Chem. Lett.* **2020**, 31, 673–676.

53 Zheng, D.; Guo, S.; Zheng, L.; Xu, Q.; Wang, Y.; Jiang, H. Red circularly polarized luminescence from intramolecular excimers restricted by chiral aromatic foldamers. *Chem. Commun.*, **2021**, 57, 12016.
54 He, J.; Yu, M.; Pang, M.; Fan, Y.; Lian, Z.; Wang, Y.; Wang, W.; Liu, Y.; Jiang, H. Nanosized Carbon Macrocycles Based on a Planar Chiral Pseudo Meta-[2.2]Paracyclophane. *Chem. Eur. J.* **2022**, 28, e202103832.
55 Lian, Z.; He,J.; Liu, L.; Fan, Y.; Chen, X.; Jiang, H. [2,2] Paracyclophanes-based double helicates for constructing artificial lightharvesting systems and white LED device. *Nat. Commun.* **2023**, *14*, 2752.
56 Lian,Z.; Liu,L.; He, J.; Fan, S.; Guo, S.; Li, X.; Liu, G.; Fan, Y.; Chen, X.; Li, M.; Chen, C.; Jiang, H. Structurally Diverse Pyrene-decorated Planar Chiral [2,2]Paracyclophanes with Tunable Circularly Polarized Luminescence between Monomer and Excimer. *Chem. Eur.* **2023**, e202303819.
57 He, J.; Fan, Y.; Lian, Z.; Guo, S.; Wang, Y.; Jiang, H. [2.2]Paracyclophane-Based Double Helices: Tunable Circularly Polarized Luminescence Driven by Self-assembly. *Adv. Optical Mater.* **2023**, 2302221.
58 Park, J. K.; Yoon, Z. S.; Yoon, M.-C.; Kim, K. S.; Mori, S.; Shin, J.-Y.; Osuka, A.; Kim, D. Möbius Aromaticity in N-Fused [24]Pentaphyrin upon Rh(I) Metalation. *J. Am. Chem. Soc.* **2008**, 130, 6, 1824-1825.
59 Xu, Q.; Wang, C.; He, J.; Li, X.; Wang, Y.; Chen, X.; Sun, D.; Jiang, H. Corannulene-based nanographene containing helical motifs. *Org. Chem. Front.* **2021**, 8, 2970.
60 Xu, Q.; Wang, C.; Zheng, D.; He, J.; Wang, Y.; Chen, X.; Jiang, H. A Distorted Hybrid Corannulene–Dibenzobistetracene. *J. Org. Chem.* **2021**, 86, 13990-13996.
61 Xu, Q.; Wang, C.; Chen, X.; Wang, Y.; Shen, Z.; Jiang, H. Corannulene-based acenes. *Org. Chem. Front.* **2022**, 9, 4981.
62 Schmider, H. L.; Becke, A. D. Chemical content of the kinetic energy density, Journal of Molecular Structure: THEOCHEM, **2000**, pp. 51-61.
63 Gonthier, J. F.; Steinmann, S. N.; Roch, L.; Ruggi, A.; Luisier, N.; Severin, K.; Corminboeuf, C. π-Depletion as a criterion to predict π-stacking ability. *Chem. Commun.* **2012**, 48, 9239-9241.
64 Liu, Z.; Lu, T.; Hua, S.; Yu, Y. Aromaticity of Hückel and Möbius Topologies Involved in Conformation Conversion of Macrocyclic [32]Octaphyrin(1.0.1.0.1.0.1.0): Refined Evidence from Multiple Visual Criteria. *J. Phys. Chem. C.* **2019**, 123, 18593–18599.

SYNOPSIS TOC.

All-carbon nanohoops with [4n]Möbius topology via hybridizing [5]helicene and cycloparaphenylene units exhibit bright circularly polarized luminescence and Hückel aromaticity.